International Journal of Rock Mechanics & Mining Sciences 48 (2011) 888–898

Contents lists available at ScienceDirect

International Journal of Rock Mechanics & Mining Sciences

journal homepage: www.elsevier.com/locate/ijrmms

Superbrittleness of rocks and earthquake activity

B.G. Tarasov *, M.F. Randolph

The University of Western Australia, Australia

ARTICLE INFO

Article history:
Received 15 March 2010
Received in revised form
1 June 2011
Accepted 22 June 2011

Keywords:
Depth earthquake activity
Rock embrittlement
Superbrittleness
Rupture mechanism

ABSTRACT

This paper demonstrates that, in contrast to relatively soft rocks, intact hard rocks failed in mode II can increase their brittleness dramatically (hundreds of times) with rising confining stress. The brittleness variation in this case follows a typical pattern of initially increasing, reaching a maximum and then ultimately decreasing. The harder the rock, the greater is the effect of embrittlement. A shear rupture mechanism discussed in the paper shows that the embrittlement results from reduction of friction within the rupture zone with rising confining stress. Transient "negative friction", which can be generated within a certain range of confining stress renders rocks superbrittle. The similarity in variation of rock brittleness with confining stress, and aftershock activity with depth, leads to the supposition that the aftershock process can be caused by generation of new faults in the intact rock mass surrounding the main fault where superbrittle behaviour determines the depth range of earthquake activity.

1. Introduction

The variation of aftershock activity with depth typically follows a pattern of initially increasing, reaching a maximum and then ultimately decreasing [1–4]. Aftershocks normally have a spatial distribution around the main shock rupture and can occur at a significant distant from the main rupture [4–6]. Fig. 1 illustrates these features. Fig. 1a shows the depth distribution of seismic activity (number of aftershocks versus depth) for different earthquake regions [4]. Fig. 1b shows the plane of seismicity for the Borah Peak, Idaho, earthquake of 1983, with several aftershocks a distance of about 3 km from the general fault plane [4].

The modern conceptual understanding of earthquakes is based upon frictional stick-slip instability along pre-existing faults [1–8]. Increase in aftershock activity with depth is explained by experimental results showing the transition from stable (ductile) sliding along the faults at low confining pressures σ_3, to rising instability (brittleness) with increasing σ_3 [7,8]. The spatial distribution of aftershocks around the main shock fault is explained by the claim that the crust is riddled with small faults of varying orientations that are reactivated due to the stress transfer [4,9–11].

It is known that mining activity at great depth can trigger severe shear rupture rockbursts, which are seismically indistinguishable from natural earthquakes [4,12]. Fig. 1c shows a plane of seismicity caused by mining activity in the East Rand Proprietary Mines gold mine, South Africa [12]. Special studies conducted in South African mines have shown that such rockbursts are associated with spontaneous development of new large shear fractures in intact rock mass, with hypocentres located at significant distances away from the excavation [12–14]. Fig. 1c shows that dynamic events can occur at distances of up to 150 m from the excavation. Despite the obvious differences between a mainshock earthquake fault and a mining excavation, both of them represent a stress concentration within the surrounding rock mass. The observations made in mines allows the supposition that earthquake aftershocks can also result from the generation of new shear fractures in the surrounding intact rock mass, due to stress changes caused by the main shock fracture [15]. However, the problem is an apparent conflict between the observed increase in aftershock activity with depth and the general belief that intact rocks under triaxial compression (with $\sigma_1 > \sigma_2 = \sigma_3$) become less brittle with rising confining pressure σ_3 (or depth).

Analysis of the post-peak behaviour of rocks of different hardness conducted in this paper shows that, in contrast to soft rocks, hard rocks show a dramatic increase in brittleness with increasing confining pressure σ_3. The brittleness variation in this case follows a typical pattern of initially increasing, reaching a maximum and then ultimately decreasing. The harder the rock, the greater is the increase in embrittlement. We consider that the rock embrittlement is caused by a special frictionless shear rupture mechanism discussed earlier in [16–18]. In accordance with this mechanism the embrittlement results from reduction of friction within the propagating shear rupture with rising σ_3. Transient "negative friction", which can occur within a certain range of σ_3, makes rocks superbrittle. The similarity in variation of rock brittleness with σ_3 and aftershock activity with depth

* Corresponding author. Tel.: +61 8 6488 7368; fax: +61 8 6488 1044.
E-mail address: tarasov@civil.uwa.edu.au (B.G. Tarasov).

1365-1609/$ - see front matter © 2011 Elsevier Ltd. All rights reserved.
doi:10.1016/j.ijrmms.2011.06.013

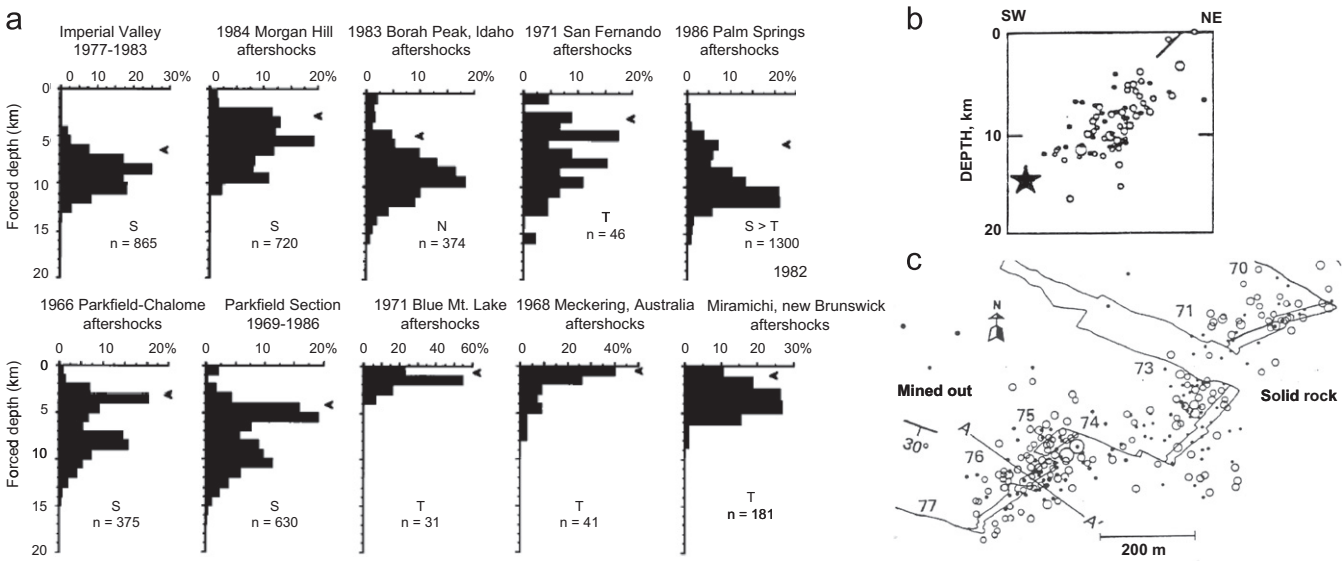

Fig. 1. (a) Earthquake depth distribution for different regions [4]. Plane of seismicity caused by: (b) the Borah Peak, Idaho, earthquake of 1983, $M=7.3$ [4] and (c) mining activity in the East Rand Proprietary Mines gold mine, South Africa (depth about 3 km) [12].

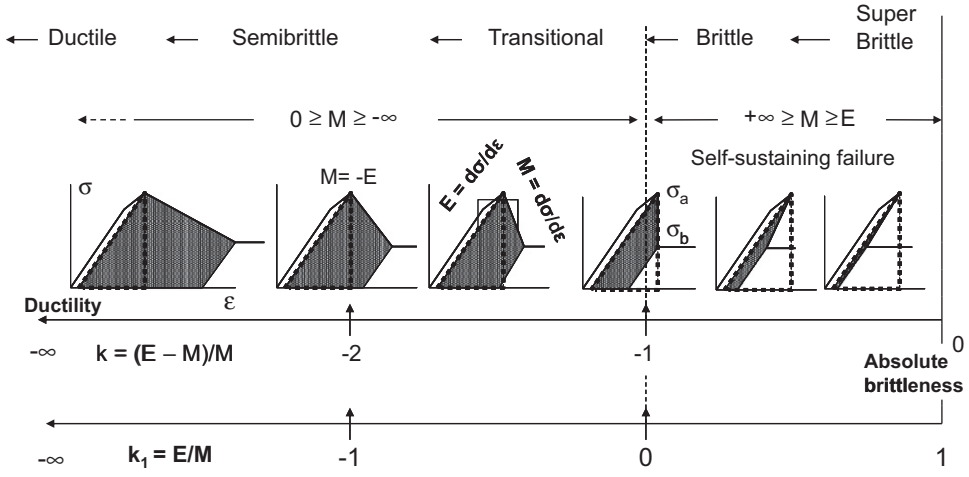

Fig. 2. Scale of brittleness index $k=(E–M)/M$ and $k_1=E/M$ with characteristic shapes of complete stress–strain curves.

suggests that the aftershock process can be caused by generation of new faults in intact rocks surrounding the main fault, with the depth range of earthquake activity determined by the stress range for superbrittle behaviour.

2. Brittleness index

Spontaneous failure, which can be treated as the manifestation of rock brittleness, takes place in the post-peak region only. Hence, post-peak energy balance of elastic and rupture energy is an essential criterion for characterisation of brittleness. To quantify rock brittleness at post-peak failure under conditions of triaxial compression ($\sigma_1>\sigma_2=\sigma_3$) we will use a brittleness index k, which characterises the capability of the rock for self-sustaining failure due to the elastic energy accumulated in the material body during loading, and which is available for rupture development in the post-peak region [18]. The index is quantified as

$$k=\frac{dW_r}{dW_e}=\frac{E-M}{M} \tag{1}$$

where $dW_r=d\sigma^2(E-M)/2EM$ is the post-peak rupture energy absorbed by the rupture process at stress degradation of the value $d\sigma$; $dW_e=d\sigma^2/2E$ is the elastic energy withdrawn from the specimen due to stress degradation of the value $d\sigma$, $d\sigma^2$ here corresponds to $(\sigma_a^2-\sigma_b^2)$—see Fig. 2 for explanation; $E=d\sigma/d\varepsilon$ is the unloading elastic modulus, $M=d\sigma/d\varepsilon$ is the post-peak modulus, and $\sigma=(\sigma_1-\sigma_3)$ is differential stress. All of these parameters can be determined from complete experimental stress–strain curves.

Fig. 2 shows the scale of rock brittleness index k with brittleness increasing from left to right. Complete curves (differential stress σ versus axial strain ε) here illustrate the variation in shape of these curves with variation in brittleness. It is supposed for simplicity that the pre-peak parts of the curves are the same. Areas restricted by dotted triangles correspond to elastic energy W_e stored within the rock material at the peak stress. Post-peak parts of the curves characterised by a post-peak modulus M are different for each curve. The shaded areas represent the post-peak rupture energy W_r associated with strength degradation at failure from the peak stress to the residual strength (horizontal part of the post-peak curves). The index k is negative, in the range

$-\infty < k < 0$, because the elastic energy is treated as positive while the rupture energy is negative.

Within the range of brittleness index $-1 < k < 0$ the elastic energy dW_e withdrawn from the material body at stress degradation on the value $d\sigma$ exceeds the corresponding rupture energy dW_r, leading to self-sustaining failure (Class II of post-peak behaviour [19]). The self-sustaining failure normally has a spontaneous character even for a hypothetically perfectly stiff testing machine. The greater the difference between dW_r and dW_e the more violent is the self-sustaining failure. At conditions of absolute brittleness $dW_r=0$, $M=E$ and $k=0$. For $k<-1$ the rupture development is not self-sustaining because the rupture energy exceeds the available elastic energy stored within the material body (Class I of post-peak behaviour [19]). Additional work must be done to cause complete failure. Variation in failure regimes with increase in rock brittleness are indicated in the upper part of Fig. 2. In addition to traditional regimes – ductile, semi-brittle, transitional and brittle – a new superbrittle failure regime is proposed. Characteristic features of this regime are discussed below. A brittleness index $k_1=E/M$, similar to $k=(E-M)/M$ can also be used for rock brittleness characterisation during post-peak failure (shown in the lower part of Fig. 2). The brittleness index k_1 represents the ratio between the released energy W_{rel} and elastic energy W_e.

3. Experimental data for increasing rock embrittlement with confining pressure

It is known that self-sustaining failure for rocks with positive post-peak modulus can be conducted in a stable manner by the use of stiff servo-controlled testing apparatus that allow the

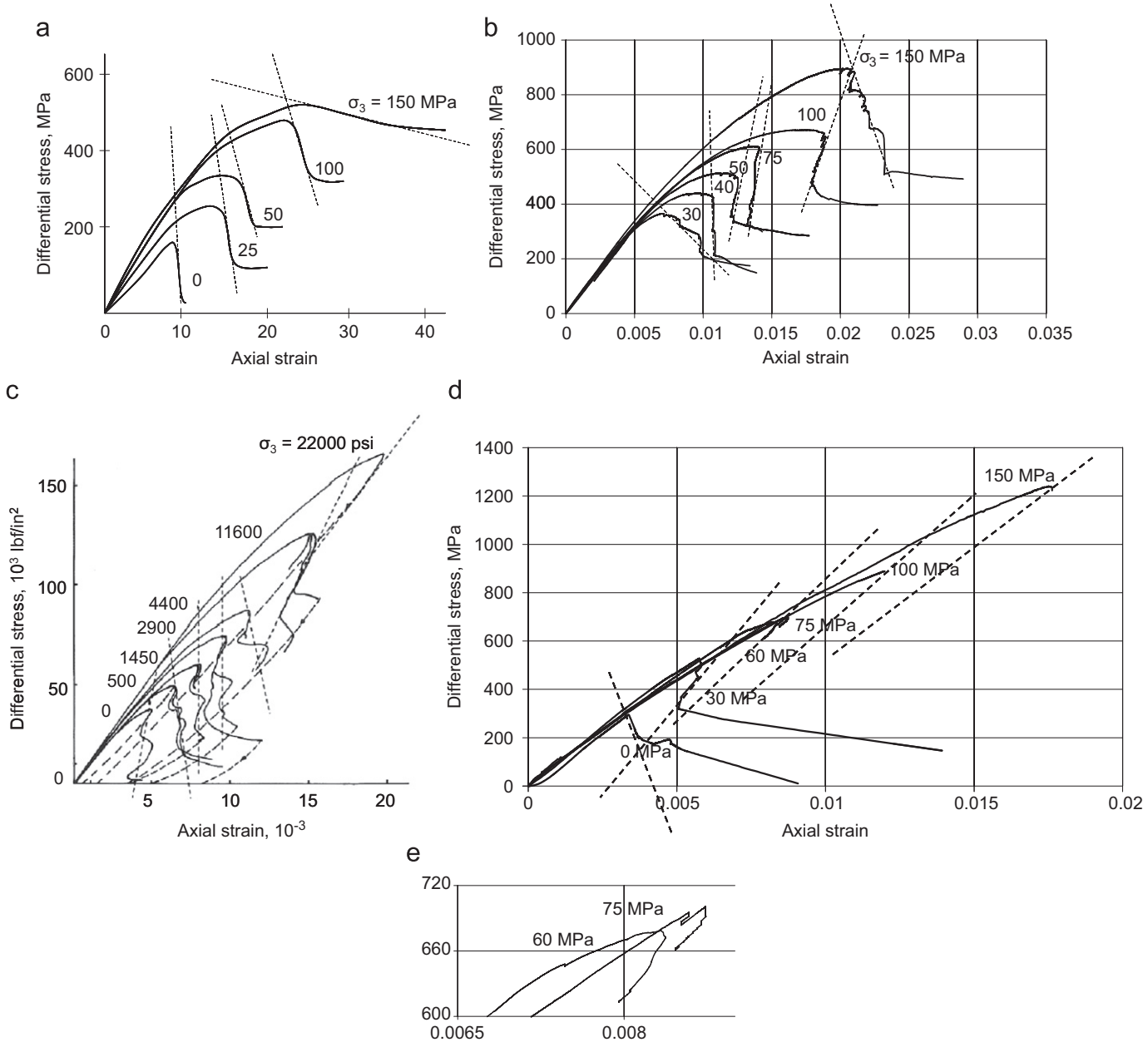

Fig. 3. Post-peak behaviour of rocks of different hardness at different levels of confining pressure σ_3: (a) sandstone [23], (b) quartzite, (c) Westerly granite [19], (d) dolerite, and (e) controlled stage of post-peak failure of dolerite specimens at $\sigma_3=60$ and 75 MPa shown on a larger scale.

excess elastic energy from the material body to be extracted by applying negative axial strains in accordance with the positive post-peak modulus M [19]. However, analysis of the available experimental data for hard rocks shows that the vast majority of results involve only the pre-peak deformation stage. Post-peak control was achieved only under uniaxial compression and at relatively low levels of confining pressures [19–22]. Increasing the confining stress (σ_3) makes the post-peak rupture control more and more difficult and finally impossible above a certain level of σ_3 [19,22]. The impossibility of rupture control at high confining pressures is usually explained as a technical problem with the apparatus, without comprehensive analysis of the situation. The analysis conducted below shows that the main reason for uncontrollable failure at high σ_3 is the extraordinary rock embrittlement and what we refer to as superbrittle behaviour. Definition for the superbrittle conditions will be given later.

Experimental results discussed below were obtained on cylindrical specimens tested in triaxial compression, $\sigma_1 > \sigma_2 = \sigma_3$, using very stiff (frame stiffness 20 MN/mm) servo-controlled testing machines [22,23]. Fig. 3 shows four sets of curves (differential stress $\sigma = (\sigma_1 - \sigma_3)$ versus axial strain ε) for rocks of different hardness (a—sandstone [23], b—quartzite, c—Westerly granite [19], and d—dolerite), with the hardness increasing from sandstone to dolerite. The hardness is estimated roughly on the basis of the average elastic modulus. All rocks were tested within the pressure range of $0 \le \sigma_3 \le 150$ MPa. Failure of all the rocks under confined conditions was by a form of shear rupture (mode II). Controllable rupture development in the post-peak region was achieved for sandstone and quartzite at all levels of σ_3. For Westerly granite rupture control was achieved for 0 psi $\le \sigma_3 \le$ 11,600 psi ($\sim$80 MPa). At σ_3=22,000 psi (152 MPa), control was possible only at the start of the post-peak stage after which explosive-like collapse of the specimens occurred. For $\sigma_3 >$ 22,000 psi (152 MPa) explosive-like uncontrollable rupture occurred at the peak stress level.

Failure of dolerite specimens was controllable for $\sigma_3 \le 30$ MPa. At greater confining pressures, 60 MPa $\le \sigma_3 \le$ 150 MPa, control was possible only at the start of the post-peak stage after which explosive-like failure took place. The controlled post-peak stage decreases with rising σ_3. Post-peak curves reflecting the controlled stage of rupture development for 60 and 75 MPa are shown in Fig. 3e on a larger scale.

To analyse the brittleness variation with rising σ_3 for the rocks presented in Fig. 3 the post-peak curves were approximated by straight lines for calculating the post-peak modulus M and brittleness index k. The lines representing the post-peak slopes for Westerly granite and dolerite tested at high σ_3 are plotted on the basis of short controlled post-peak curves.

Fig. 4 shows the variation of brittleness index k with confining pressure σ_3 for the rocks discussed, with brittleness increasing from left to right. The graph for sandstone shows that increase in σ_3 makes the rock less brittle. This behaviour is typical for soft and insufficiently hard rocks. For the quartzite, increase in σ_3 within the range of 0–100 MPa makes it more brittle. At greater σ_3 the brittleness decreases. The graphs for granite and dolerite show very severe rock embrittlement. At σ_3=75 MPa the dolerite became 250 times more brittle compared with uniaxial compression ($k_o = -1.5$; $k_{75} = -0.006$). At σ_3=100 and 150 MPa the brittleness increased significantly, further approaching absolute brittleness (k=0). The dashed lines indicate the expected brittleness variation for granite and dolerite at greater σ_3: the brittleness continues to increase until it reaches a maximum at some level of σ_3 and than decreases since all rocks become ductile at very high σ_3. For less hard rocks (such as the quartzite) the mode of brittleness variation is similar but the maximum brittleness is lower and the range of confining pressure where embrittlement takes place is smaller. The self-sustaining failure regime corresponds to $-1 < k < 0$.

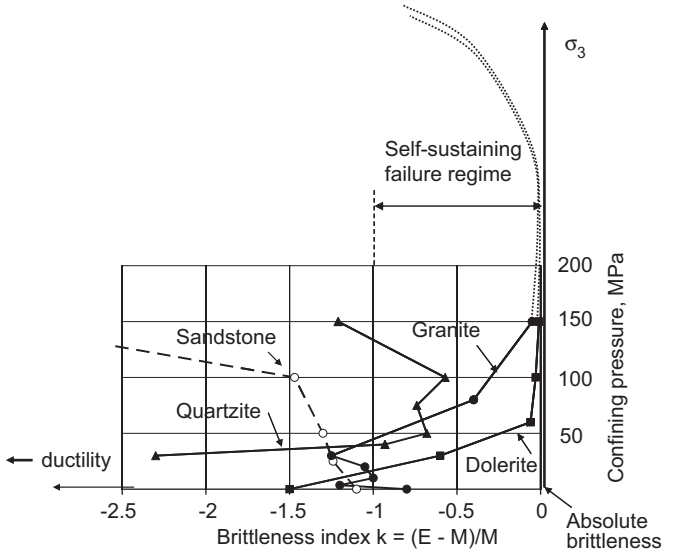

Fig. 4. Variation of brittleness index k versus confining pressure σ_3 for rocks of different hardness (modified from [18]).

4. Mechanism of rock embrittlement at high confining pressures

4.1. Frictionless model of primary ruptures

The mechanism of rock embrittlement discussed below is based upon modern understanding of shear fracture development. It is known that a shear rupture can propagate in its own plane due to creation of short tensile cracks in front of the rupture tips [15,24,25]. This forms the universal structure of shear ruptures represented by an echelon of blocks (or slabs) separated by tensile cracks—known as 'book-shelf' structure [15,24–27]. The initial angle β_o of the tensile crack and block inclination to the shear rupture plane is about 30°–40° [28]. Shear displacement along the fault causes rotation of the blocks of the 'book-shelf' structure between the rupture surfaces [24–27].

Fig. 5a illustrates the essence of the shear rupture mechanism according to modern understanding. All existing shear rupture models consider shear displacement of the fault faces in the fault head as a frictional process (e.g. [15,24–27]). It is assumed that the blocks of the 'book-shelf' structure formed at the fault tip collapse during rotation creating friction within the fault head. A graph under the shear rupture in Fig. 5a shows the shear resistance variation along the fault head. The cohesive strength τ_{coh} and the initial resistance caused by the front blocks are substituted gradually by frictional resistance due to block collapse. At the end of the rupture head the resistance reaches the minimum value, which is determined by friction τ_f.

In accordance with this model any increase in σ_3 increases the friction within the rupture zone including the rupture head, which must be followed by an increase in rupture energy and decrease in brittleness. The question is: what kind of changes in the described rupture mechanism can cause the observed very severe embrittlement of rocks?

It is known that increase in σ_3 makes tensile cracks and, consequently, rotating blocks shorter. We can suppose that at special levels of σ_3 the blocks can become short enough to withstand rotation without collapse, thus operating as hinges.

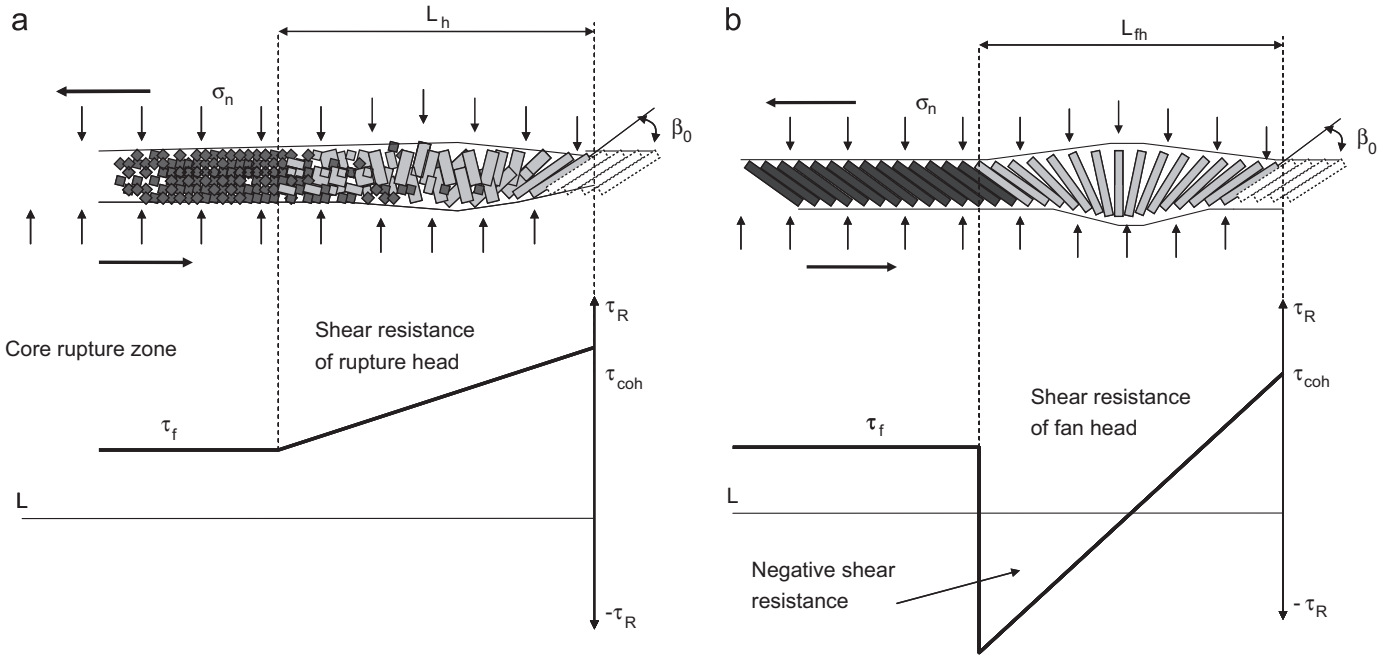

Fig. 5. Shear rupture mechanisms: (a) common frictional and (b) new frictionless models.

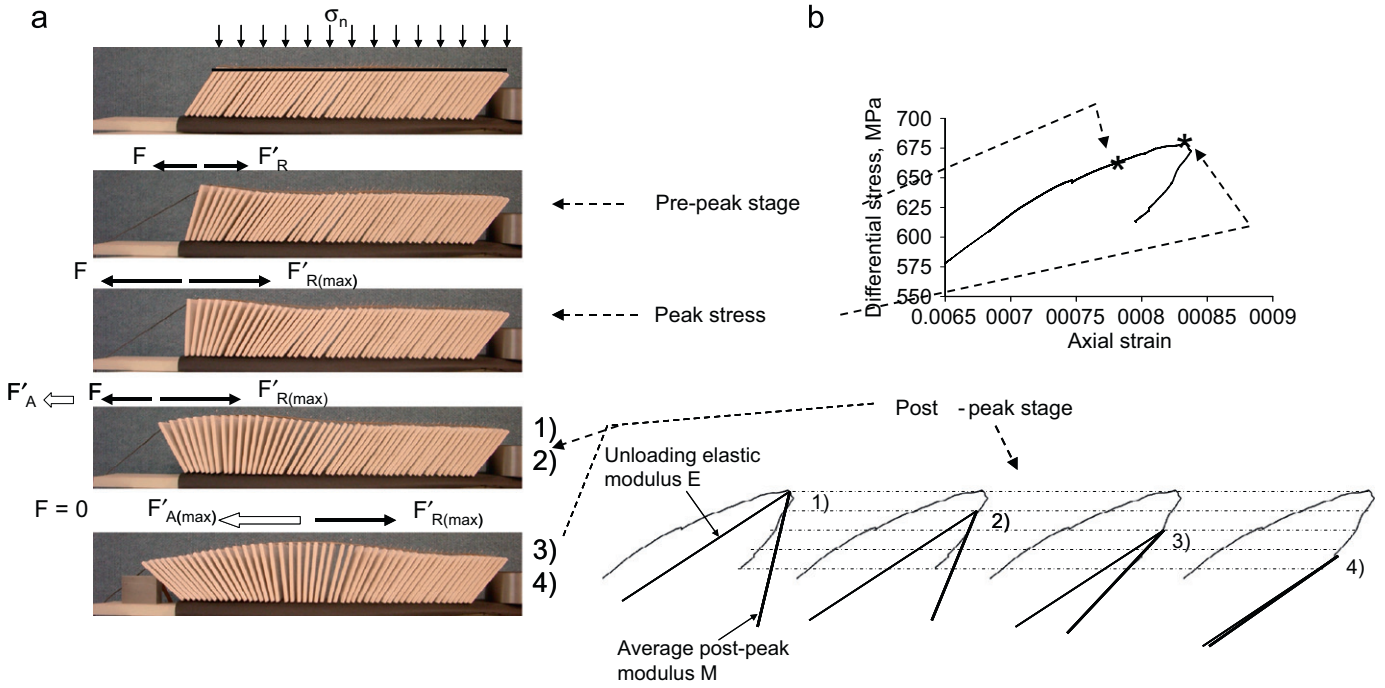

Fig. 6. (a) A physical model of the fan head formation. (b) Fragment of stress–strain curve for dolerite specimen tested at $\sigma_3 = 60$ MPa.

This can only happen in hard rocks because very strong material is required to achieve this. The very high strength of the rotating blocks is provided also by a scale effect: the smaller the rock fragment (rotating block) the stronger it is. The thickness of shear ruptures in experiments showing high brittleness was less than 0.1 mm [16], which suggests that the dimensions of the rotating blocks involved in these shear ruptures should be about the same order.

Fig. 5b illustrates a model where rotating blocks behave as hinges. Due to consecutive formation (by splitting) and rotation of the blocks, these should form a fan structure within the rupture head. A remarkable feature of the rotating blocks (hinges) in the second half of the fan structure (where $\beta > 90^\circ$) is the creation of active forces (see explanation below on the basis of Fig. 6). A graph under the shear rupture in Fig. 5b shows the shear resistance variation along the fault head. The bottom part of the graph represents active forces (negative resistance) acting in the second half of the head and assisting the fault displacement. We refer to the negative resistance symbolically as 'negative friction'. In the core zone represented by blocks that have completed their rotation the normal residual friction is restored.

A physical model in Fig. 6 illustrates features of the fan head formation. All blocks of the model are confined by two elastic belts (on top and bottom) representing material of the rupture

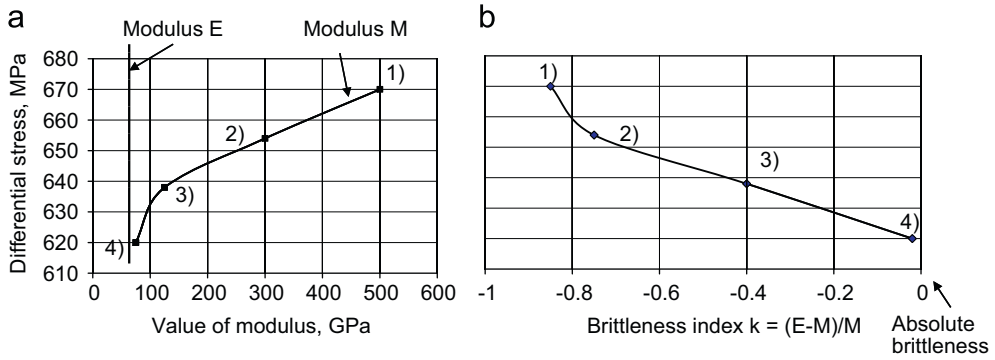

Fig. 7. Variation of (a) post-peak modulus M and (b) brittleness index $k=((E-M)/M)$ versus differential stress σ for dolerite specimen failed at $\sigma_3=60$ MPa [18].

faces. Normal stress σ_n is applied to the structure. This model introduces key roles of elasticity of the face material and normal stress in the fault structure development. Due to elasticity of the face material the rotating blocks are separated from the intact material and rotated sequentially under the effect of applied shear force F, forming a fan-shaped structure. The picture illustrates different stages of the fan head formation. The forces shown indicate schematically the variation in total shear resistance of the growing rupture head (here, F is the applied force; F'_R and F'_A are reactive and active forces). The forces F'_R and F'_A are functions of normal stress σ_n, elasticity of the face material and geometrical characteristics of the rotating blocks (see more details in [17,18]). During formation of the first half of the fan head the shear resistance increases and reaches maximum, F'_{Rmax}, at the moment when the first half of the fan structure is formed. This rupture process takes place during the pre-peak stage of the material loading. Acoustic emission studies show that for hard rocks the localised shear fracture development starts close to the peak strength [25,29]. Unlike relatively soft rocks where intensive distributed microcracking precedes the rupture localisation for hard rocks the localised shear fracture development can occur practically without distributed microcracking [25,29]. In the model the microcracking process is associated with tensile crack formation causing separation of the rotating blocks from the intact rock mass in the rupture tip.

Thanks to the creation of an active force F'_A at formation of the second half of the head, the total shear resistance of the fan head decreases. This happens due to the effect of normal stress σ_n and elastic forces in the face material on blocks positioned at angles $\beta > 90^\circ$. Elastic energy accumulated within the face material in the first half of the fan head is released in the second half. Decrease in resistance of the fan-head structure corresponds to the start of the post-peak deformation stage. At completion of the fan-structure formation the value of the active force becomes equal to the reactive force $F'_{Amax}=F'_{Rmax}$. Thus the fan structure represents a self-equilibrating mechanism and can move spontaneously as a wave with very small shear resistance.

In the idealised fan-head model the resistance to rupture propagation is determined only by the tensile strength of the material associated with consecutive formation of blocks in front of the propagating rupture. It is important that the fan head can propagate independently of the core zone, which can remain immobile due to high frictional resistance. In this situation the rupture energy is determined by shear resistance of the fan head only. The fan-head rupture mechanism represents the most energy efficient shear rupture mechanism.

This model explains the reason for the impossibility of controlling rupture beyond a certain stage of the post-peak deformation, as observed at high σ_3. To analyse this we may divide the post-peak curve obtained for the dolerite specimen at $\sigma_3=60$ MPa into four stages with equal intervals of differential stress (Fig. 6b bottom). Each stage is characterised by average values of unloading elastic modulus E and post-peak modulus M. It is assumed that modulus $E=84{,}000$ MPa is constant for all four stages due to relatively small stress degradation between the peak stress and the point of instability start. During the rupture development from stage (1) to stage (4), modulus M decreases, approaching modulus E. At stage (4) levels of post peak modulus ($M=84{,}500$ MPa) and elastic modulus ($E=84{,}000$ MPa) become very close. Areas located between the E and M lines represent the post-peak rupture energy dW_r which decreases dramatically with the rupture development. Theoretically at $M=E$ the rupture energy becomes equal to zero and material exhibits absolute brittleness. Decrease in rupture energy is associated with development of the second half of the fan head.

Fig. 7 shows variations of modulus E and M and brittleness index k versus differential stress σ for the same dolerite specimen. At stages (1) and (4) values of the brittleness index are –0.85 and –0.006, resepctively. We can suppose that after stage (4) formation of the fan head is complete and the head starts to propagate spontaneously as a wave, independently on the rupture core, rendering further rupture control impossible. Experiments conducted on the physical fan-head model showed that the length of the fan head is a function of the normal stress σ_n. Increase in σ_n reduces the fan head length. This explains why the controllable stage of the post-peak deformation decreases with increase in σ_3.

4.2. Frictionless model of complex shear ruptures

Generally faults represent complex formations involving relatively wide rupture zones of crushed rock, which implies very high rupture energy and, consequently, relatively low brittleness. However, a specific rupture mechanism governing the fault development provides frictionless rupture conditions within the fault zone at different stages of the fault development, which makes the failure process very brittle. This mechanism is discussed below.

It is known that segmentation is a fundamental feature of fault development [4,30–34]. A similar segmented structure of fault zones extends throughout the seismogenic depth, deeper that 10 km in the earth's crust [33,34]. Faults are composed of essential structural elements: fault segments with an en echelon array and fault jogs (overlap zones). Laboratory experiments [35] have demonstrated that fault development can result from consecutive advanced triggering of new shear fractures (new segments) in front of the propagating fault. The triggering is caused by the stress transfer ahead of the fault through rock mass already stressed close to failure. The fault and segments propagating toward each other form jogs (overlap zones) where they meet. Analysis of the segmented fault structure formed under

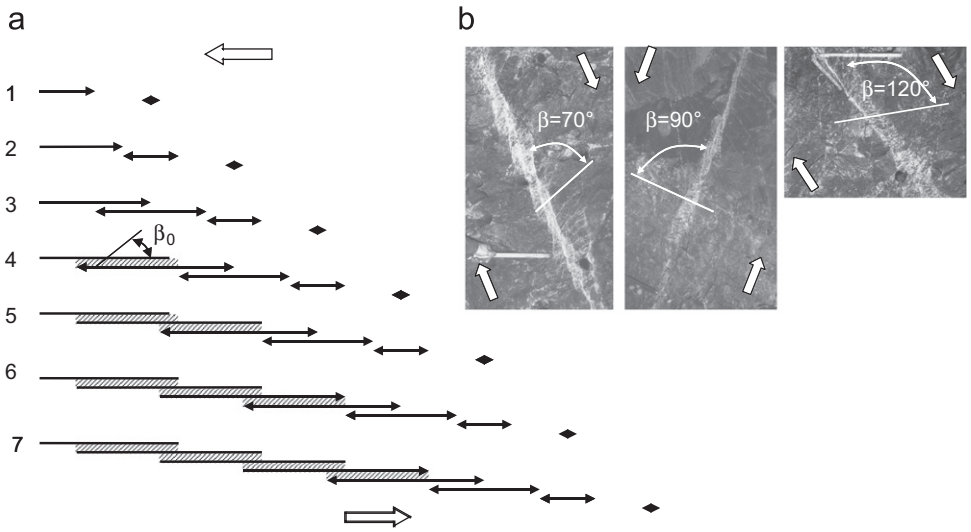

Fig. 8. (a) Model of fault propagation due to consecutive triggering of new advanced segments, which form at linkage overlap zones with 'book-shelf' structure. (b) Natural faults [13] illustrating rotation of blocks of the book-shelf structure at fault displacement.

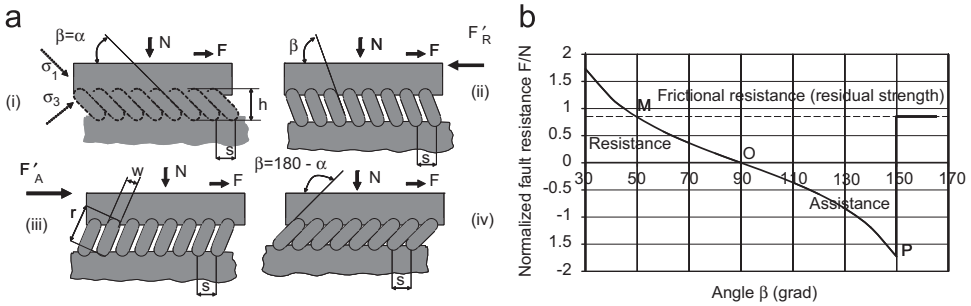

Fig. 9. (a) Model of fault displacement accompanied by rotation of blocks of the book-shelf structure. (b) Normalised fault shear resistance F'/N versus angle β at the fault displacement (from [16]).

conditions of high confining pressures or great depths suggests that formation of compressional type of jogs predominates under highly confined conditions [13,35]. A possible reason for that is discussed in [18].

Fig. 8 shows seven steps of the fault development in accordance with the 'advance triggering' segmentation mechanism [17]. The fault propagates from left to right. Solid arrows represent segments; hollow arrows show directions of the applied shear stress. The segments form compressional overlap zones on meeting. When the extending overlap zone in hard brittle rocks reaches some critical length it fractures dynamically into an echelon of rotating blocks forming the book-shelf structure. The book-shelf structure represents a fundamental feature of any shear fracture (fault). The initial orientation of tensile cracks separating the blocks coincides with the direction of the major compressive stress (β_o=30°–40°) [28]. The overlap zones, by joining, can form long faults involving book-shelf structures. Photographs of such shear fractures with the book-shelf structure caused severe rockbursts in deep South Arican mines are shown in Fig. 8b [13]. The photographs show also that displacement along the fault is accompanied by rotation of the blocks (β=70°, 90°, 120°). In special cases discussed below the rotating blocks can operate as hinges decreasing dramatically the shear resistance of the fault.

An idealised fault model involving an echelon of rotating blocks is shown in Fig. 9a [16]. Shear F and normal N forces are applied to the model. Fig. 9b illustrates the variation in normalised fault resistance F/N as the angle β increases during shear displacement of the fault. The resistance decreases, reaching zero at β=90°, beyond which it becomes negative (releasing energy). The negative resistance ('negative friction') is provided by the normal force N (function of σ_3) existing across the fault, which encourages block rotation beyond β=90°, consequently assisting the fault displacement. This mechanism makes the material extremely brittle, because of the loss of any positive resistance over a finite displacement until the restoration of frictional resistance once the blocks have completed their rotation.

To understand correctly the role of the book-shelf structure in rock embrittlement it is necessary to take into account also the following features of segmented faults observed experimentally [35]: (1) faults are multi-hierarchical formations; (2) once a number of segments of a given hierarchical rank coalesce, they behave as a whole as a new and longer segment of one higher rank; (3) segments of higher rank can trigger a new segment (rupture) at greater distance; and (4) the new triggered segment starts as a primary rupture.

Fig. 10 shows schematically three stages associated with development of three types of segments of different rank. Shear stress direction here is indicated by open arrows, the fault propagating from left to right. The fault nucleates as a primary rupture because the self-equilibrating fan-head mechanism mobilised in very thin primary ruptures is the most energy efficient shear rupture mechanism. When the primary rupture becomes sufficiently long a new primary rupture (segment) can be triggered in front of the current one at a distance x_I due to stress transfer. Further propagation of these ruptures can trigger the third one and so on. On meeting, these ruptures play a role of segments of rank-I and form corresponding overlap zones with the book-shelf structure. After joining of a number of segments of

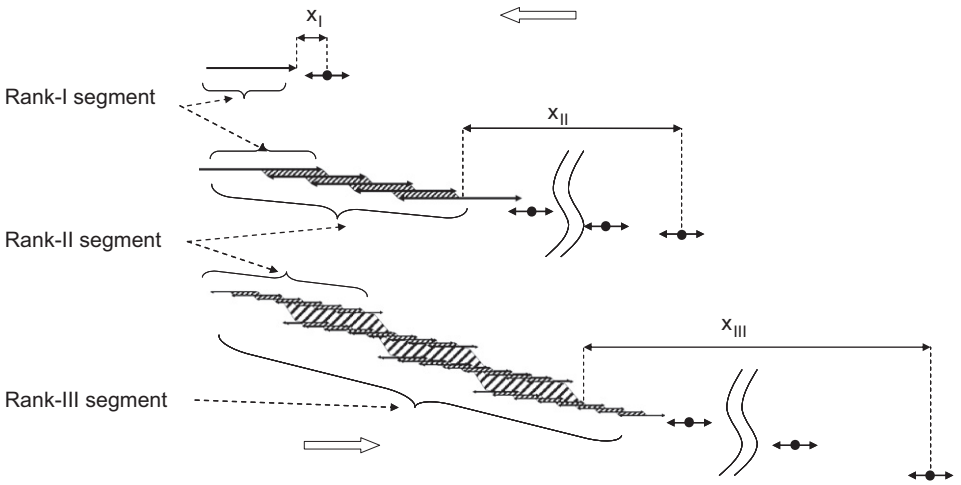

Fig. 10. Evolution of fault structure with development of segments of different ranks (multi-hierarchical structure).

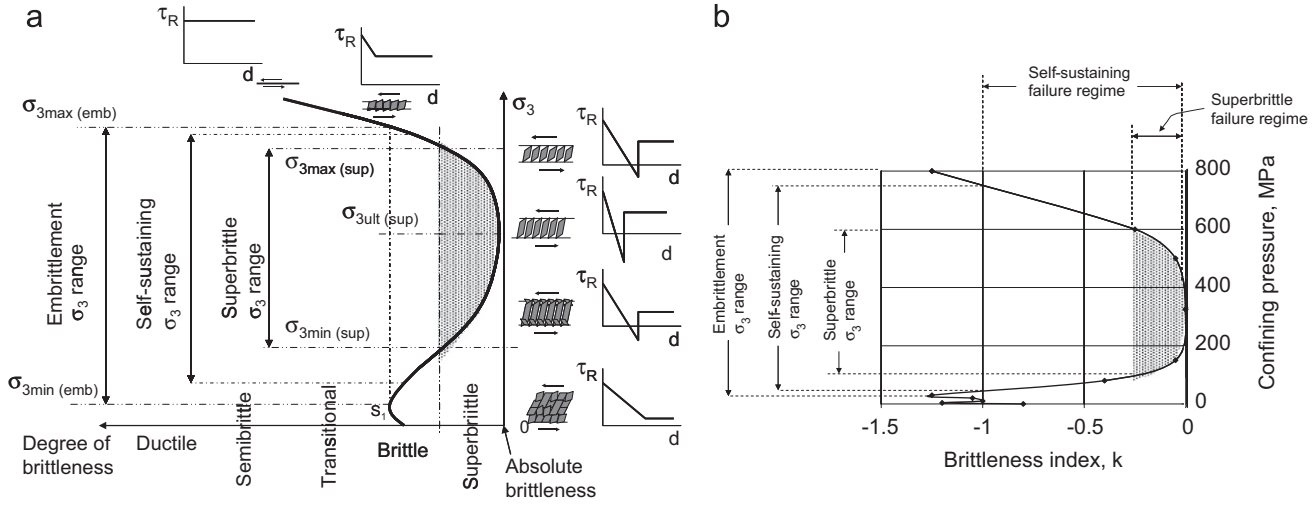

Fig. 11. (a) Model of brittleness variation versus confining pressure σ_3. (b) Estimated variation of brittleness index k versus confining pressure for Westerly granite.

rank-I the combined formation starts behaving as a segment of higher rank-II. The rank-II segment can trigger a series of new primary ruptures at different distances with maximum remoteness of x_{II}. The key feature of fault segmentation is the fact that a new segment triggered by the current segment of any rank nucleates as a primary rupture (due to the most energy efficient shear rupture mechanism). At its propagation towards the current segment (and in the opposite direction) the new segment will be subjected to similar evolution as occurred for the current segment. After linkage of a number of rank-II segments due to creation of corresponding overlap zones with the book-shelf structure, the next rank-III segment will be formed (shown on a smaller scale $\approx$ 1:5). Further development of this fault will be accompanied by creation of higher rank segments.

The most important feature of the fault structure evolution relevant to the main subject of this paper is the fact that low rank segments with corresponding book-shelf structure represent basic elements of any higher rank segment for any fault (including very large ones). At fault development, frictionless conditions can be provided first of all in low rank segments where relatively small displacement is required to rotate blocks of the book-shelf structure up to angle $\beta > 90^\circ$. Once frictionless conditions have been reached, displacement along the low rank segments occurs extremely violently. Relatively thin localised zones of very intense destruction can be observed in practise in each fault. The initial frictionless structure of these segments is completely destroyed by explosive-like extensive shear, creating gouge material. Higher rank segments with the book-shelf structure, where blocks rotate with angle $\beta < 90^\circ$, serve as a damping mechanism accommodating large fault displacement. Hence, we can suppose that low rank segments are responsible for high rock brittleness at the fault development.

It is important to note that the frictionless mechanism activated in primary fractures and in segmented faults do not affect the initial and the frictional residual rock strength (and consequently the Mohr–Coulomb criterion). The frictionless behaviour manifests itself transiently during failure in the post-peak region between the peak and residual strength.

5. Model of brittleness variation with confining pressure

Now we can discuss the reason for the specific rock brittleness variation with confining pressure shown in Fig. 4. Let us consider first the variation in brittleness versus confining pressure σ_3 on the basis of experimental results presented in Fig. 4 for Westerly granite and dolerite. Fig. 11a illustrates this variation schematically. The horizontal axis here represents the degree of brittleness and involves four traditional categories (brittle, transitional, semibrittle, and ductile) as well as a new one—superbrittle. Fig. 11a explains the essence of the rock brittleness variation with σ_3,

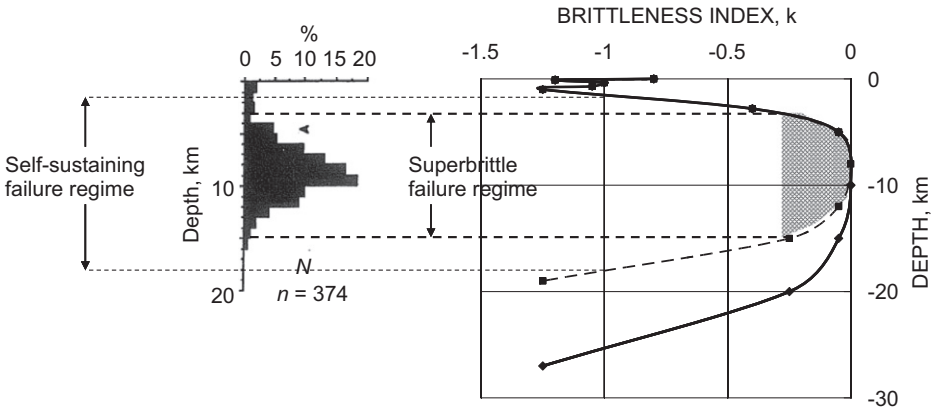

Fig. 12. Depth distribution of aftershock activity for the Borah Peak, Idaho, earthquake [4] and variation of brittleness index k with depth for Westerly granite.

showing fragments of shear ruptures with characteristic features of the fault structure (book-shelf structure). Within the range of confining pressure $0–\sigma_{3min(emb)}$ the brittleness variation can accord with the commonly accepted frictional model due to collapsing of the long rotating blocks (curve S_1 observed for Westerly granite). Within the embrittlement pressure range, $\sigma_{3min(emb)}–\sigma_{3max(emb)}$, due to shortening of the rotating blocks, the frictionless mechanism is activated, increasing the rock brittleness compared with the frictional rupture mechanism. The efficiency of the frictionless mechanism is determined by how perfect and uniform the fault structure is. At the low end of the embrittlement pressure range, when the relative length (length/thickness) of the rotating block is still large, the blocks are subjected to partial destruction (buckling) as they rotate. At higher σ_3, with shorter blocks, this imperfection decreases, rendering the frictionless mechanism more efficient. The optimal efficiency takes place at $\sigma_{3ult(emb)}$ when the blocks rotate with minimum destruction making the material ultimately brittle. At greater σ_3 the efficiency reduces because shorter blocks gradually lose any potential for creating negative resistance from rotation. Finally very short blocks lose this capability completely and the rock behaviour returns to the commonly accepted frictional mode. Idealised stress-displacement curves on the right illustrate evolution of the rupture resistance with displacement for different conditions of the rotating blocks, showing the negative shear resistance occurring over a certain σ_3 range.

In accordance with this model of rock embrittlement, two specific zones of confining pressure σ_3 can be distinguished. (1) *Embrittlement pressure range* ($\sigma_{3min(emb)}–\sigma_{3max(emb)}$)—a zone where the frictionless mechanism is activated decreasing the frictional rupture resistance. (2) *Superbrittle pressure range* ($\sigma_{3min(sup)}–\sigma_{3max(sup)}$)—a zone where the frictionless mechanism is capable of creating 'negative friction'. This zone is shown by the shaded area. It should be noted that the superbrittle failure regime represents the most brittle form of the self-sustaining failure regime.

Using experimental data we can estimate very roughly stress boundaries for embrittlement ($\sigma_{3min(emb)}$, $\sigma_{3max(emb)}$) and superbrittle behaviour ($\sigma_{3min(sup)}$, $\sigma_{3max(sup)}$) for Westerly granite. The lower limit for embrittlement $\sigma_{3min(emb)} \approx 30$ MPa corresponds to the confining pressure from which rock brittleness starts to increase. The lower limit for superbrittle behaviour $\sigma_{3min(sup)} \approx 100$ MPa corresponds approximately to the confining stress at which rupture control becomes impossible (when the effect of 'negative friction' comes into play). What is the upper level, $\sigma_{3max(emb)}$, at which the frictionless mechanism should be suppressed and the rupture mechanism return to the commonly assumed frictional response? We can estimate this on the basis of the following experimental results obtained on hard rocks [36]. An important change in the fracture mechanism was observed experimentally by Shimada [36] at the level of confining pressure when the cohesive strength equals the frictional strength. Two types of brittle fracture, 'low-pressure' and 'high-pressure' types, were distinguished:

(1) The low-pressure type fracture occurs when the cohesive strength is higher than the frictional strength, the main features being: (a) numerous microcracks and crushed zones associated with the main fault, which is oriented at 15°–40° to the major stress σ_1 direction, and (b) rapid increase in acoustic emission (AE) as a final explosive-like fracture is approached.
(2) The high-pressure type fracture occurs when the cohesive strength is lower than the frictional strength, with characteristic features being: (a) there are fewer microcracks in total and they are not concentrated close to the main fault but are homogeneously distributed throughout the specimen, suggesting that cataclastic ductile flow could occur; (b) AE activity remains constant followed by a sudden final fracture; and (c) the main fault is sharp and oriented at approximately 45° to the compressive stress σ_1 direction.

It is known that AE events in a brittle rock mainly correspond to the generation of microcracks. The frictionless mechanism discussed above is associated with intensive microcracking in the fan head before instability, and in the head and overlap zones during instability. At high $\sigma_3 > \sigma_{3max(emb)}$ the frictionless mechanism is substituted by a frictional shear rupture mechanism that cannot generate such AE activity. On the basis of the above experiments we can suppose that the frictionless ruptures described here correspond to a form of low-pressure rupture. It is established that at room temperature the confining pressure boundary between low- and high-pressure ruptures corresponds to 800 MPa for Mannari granite [36]. This pressure level can be considered as the high pressure boundary ($\sigma_3 = \sigma_{3max(emb)}$) for the frictionless mechanism in this rock at room temperature. The high pressure boundary for superbrittle rock behaviour ($\sigma_3 = \sigma_{3max(sup)}$) should be lower. Special experimental studies are needed to study this question. Here we estimate arbitrarily the high pressure boundary for superbrittle behaviour for Mannari granite as $\sigma_{3max(sup)} \approx 600$ MPa. Westerly granite has similar mechanical properties to Mannari granite [36]. Hence, we can suppose that for Westerly granite boundary levels of confining pressure are: $\sigma_{3min(emb)} \approx 30$ MPa, $\sigma_{3max(emb)} \approx 800$ MPa, $\sigma_{3min(sup)} \approx 100$ MPa and $\sigma_{3max(sup)} \approx 600$ MPa. Fig. 11a shows variation of brittleness index k versus confining pressure σ_3 for Westerly granite in accordance with the above estimations. The granite should exhibit maximum brittleness at about $\sigma_{3ult(sup)} \approx 300$ MPa.

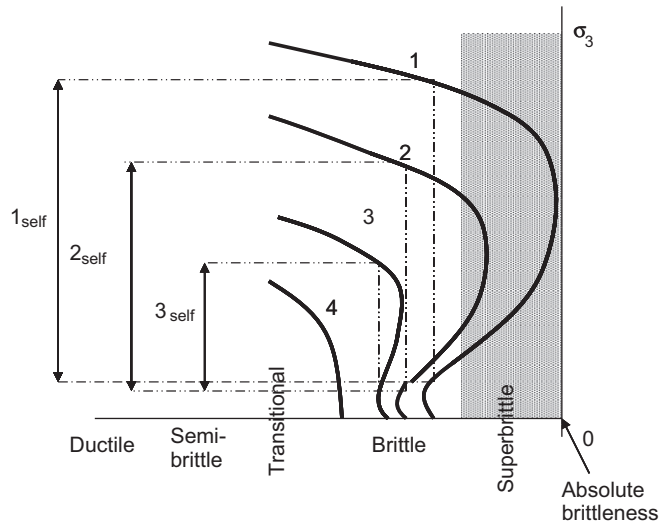

Fig. 13. Theoretical curves illustrating brittleness variation for four rocks of different hardness and different capability to embrittlement (modified from [18]).

A graph in Fig. 12 illustrates these results as applied to the earth's crust. The possible effect of elevated temperature on the frictionless mechanism activity is taken into account, decreasing levels of the high pressure boundaries $\sigma_{3max(emb)}$ and $\sigma_{3max(sup)}$. This is done arbitrarily due to the lack of any experimental information in this regard. A probable zone of superbrittle rock behaviour is indicated on the graph. Fig. 12 shows that the character of rock brittleness variation with depth is comparable with the typical variation of earthquake activity illustrated by the Borah Peak, Idaho, earthquake of 1983 [4]. The similarity in variation of rock brittleness and aftershock activity with depth suggests that the aftershock process may be caused by the generation of new faults in intact rock mass surrounding the main fault, with the depth range of earthquake activity determined by the stress range for superbrittle behaviour.

Fig. 13 shows theoretical curves illustrating brittleness variation for four rocks of different hardness (in accordance with Fig. 4). The hardness increases from rock 1 to rock 4. The embrittlement pressure range for rocks 1, 2, and 3 are indicated in the picture. The softer the rock the less embrittlement occurs. Soft rock (4) with normal frictional rupture mechanism does not exhibit embrittlement at all. Different ranges of confining pressure where different rocks exhibit embrittlement can explain the different depth ranges of aftershock activity presented in Fig. 1.

6. Conclusions

This paper proposes a new approach for explanation of the specific variation of aftershock activity with depth. Previously unexplored properties of hard rocks – increase in brittleness with rising confining pressure with superbrittle behaviour for conditions corresponding to the depth of maximum earthquake activity – give grounds to suppose that earthquake depth activity reflects rock brittleness variation with depth. Other key conclusions are:

- The paper proposes specific brittleness indexes to estimate rock brittleness during post-peak failure.
- Characteristic features of superbrittle conditions are defined.
- Experimental results obtained for rocks of different hardness show that the effect of rock embrittlement due to confining pressure increases with increase of rock hardness.
- A mechanism causing rock embrittlement with rising confining pressure is proposed.
- The new approach allows better understanding of the mechanics of deep seated dynamic events such as earthquakes and shear rupture rockbursts.

Acknowledgements

This work has been supported over a number of years by the Centre for Offshore Foundation Systems (COFS) at the University of Western Australia, which was established under the Australian Research Council's Special Research Centre scheme and is now supported by the State Government of Western Australia through the Centre of Excellence in Science and Innovation program. This support is gratefully acknowledged.

References

[1] Sibson RH. Fault zone models, heat flow, and the depth distribution of earthquakes in the continental crust of the United States. Bull Seismol Soc Am 1982;72:151–63.
[2] Marone C, Scholz CH. The depth of seismic faulting and the upper transition from stable to unstable slip regimes. Geophys Res Lett 1988;15:621–4.
[3] Duebendorfer EM, Vermilye J, Geiser PA, Davis TL. Evidence for aseismic deformation in the western transverse ranges, Southern California: implications for seismic risk assessment. Geology 1998;26(3):271–4.
[4] Scholz CH. The mechanics of earthquakes and faulting. Cambridge: Cambridge University Press; 2002.
[5] Tajima F, Kanamori H. Global survey of aftershock area expansion patterns. Phys Earth Planet Int 1985;40:77–134.
[6] Mendoza C, Hartzell SH. Aftershock patterns and main shock faulting. Bull Seismol Soc Am 1988;78:1438–49.
[7] Brace WF, Byerlee JD. Stick slip as a mechanism for earthquakes. Science 1966;153:990–2.
[8] Byerlee JD, Brace WF. High-pressure mechanical instability in rocks. Science 1969;164:713–5.
[9] Stain RS. The role of stress transfer in earthquake occurrence. Nature 1999;402:605–9.
[10] King GCP, Cocco M. Fault interaction by elastic stress changes: new clues from earthquake sequences. Adv Geophys 2000;44:1–38.
[11] Hough SE. Earthshaking science. Princeton: Princeton University Press; 2002.
[12] McGarr A. Some applications of seismic source mechanism studies to assessing underground hazard. In: Mines NC Cay, Wainwright EH, editors. Proceedings of the 1st international congress on rockbursts & seismicity; 1984. p. 199–208.
[13] Ortlepp WD. Rock fracture and rockbursts. Johannesburg: South African Institute of Mining and Metallurgy; 1997.
[14] Ortlepp WD. Note on fault-slip motion inferred from a study of microcataclastic particles from an underground shear rupture. Pure Appl Geophys 1992;139:677–95.
[15] Reches Z. Mechanisms of slip nucleation during earthquakes. Earth Planet Sci Lett 1999;170:475–86.
[16] Tarasov BG, Randolph MF. Frictionless shear at great depth and other paradoxes of hard rocks. Int J Rock Mech Min Sci 2008;45:316–28.
[17] Tarasov BG. Intersonic shear rupture mechanism. Int J Rock Mech Min Sci 2008;45:914–28.
[18] Tarasov BG. Superbrittleness of rocks at high confining pressure. In: Proceedings of the 5th International seminar on deep & high stress mining; 2010. p. 119–33.
[19] Wawersik WR, Brace WF. Post-failure behavior of a granite and diabase. Rock Mech 1971;3:61–85.
[20] Lockner DA, Byerlee JD, Kuksenko V, Ponomarev A, Sidorin A. Quasi-static fault growth and shear fracture energy in granite. Nature 1991;350:39–42.
[21] Lockner D. The role of acoustic emission in the study of rock fracture. Int J Rock Mech Min Sci Geomech Abstr 1993;30(7):883–99.
[22] Tarasov BG, Dyskin AV. The phenomenon of anomalous rock embrittlement. In: Proceedings of the 6th international symposium on rockburst & seismicity in mines; 2005. p. 311–7.
[23] Stavrogin AN, Tarasov BG. Experimental physics and rock mechanics. Rotterdam: Balkema; 2001.
[24] Cox SJD, Scholz CH. On the formation and growth of faults: an experimental study. J Struct Geol 1988;10:413–30.
[25] Reches Z, Lockner DA. Nucleation and growth of faults in brittle rocks. J Geophys Res 1994;99:18159–73.
[26] Peng S, Johnson AM. Crack growth and faulting in cylindrical specimens of Chelmsford granite. Int J Rock Mech Min Sci 1972;9:37–86.
[27] King GCP, Sammis CG. The mechanisms of finite brittle strain. Pure Appl Geophys 1992;138(4):611–40.

[28] Horii H, Nemat-Nasser S. Compression-induced microcrack growth in brittle solids: axial splitting and shear failure. J Geophys Res 1985;90:3105–25.
[29] Lei X, Kusunose K, MVMS Rao, Nishizawa O, Satoh T. Quasi-static fault growth and cracking in homogeneous brittle rock under triaxial compression using acoustic emission monitoring. J Geophys Res 2000;105:6127–39.
[30] Segall P, Pollard DD. Mechanics of discontinuous faults. J Geophys Res 1980;85:555–68.
[31] Aydin A, Schultz RA. Effect of mechanical interaction on the development of strike-slip faults with echelon patterns. J Struct Geol 1990;12:123–9.
[32] De Joussineau G, Aydin A. Segmentation along strike-slip faults revisited. Pure Appl Geophys 2009;166:1575–94.
[33] Li YG, Vidale JE, Aki K, Marone CJ, Lee WHK. Fine structure of the Landers zone: segmentation and the rupture process. Science 1994;256:367–70.
[34] Nishigami K. Deep crustal heterogeneity along and around the San Andreas fault system in central California and its relation to the segmentation. J Geophys Res 2000;105:7983–98.
[35] Otsuki K, Dilov T. Evolution of hierarchical self-similar geometry of experimental fault zones: Implications for seismic nucleation and earthquake size. J Geophys Res 2005;110:B03303.
[36] Shimada M. Mechanical behaviour of rocks under high pressure conditions. Rotterdam: Balkema; 2000.